Optimized Control of DFIG-Based Wind Generation Using Sensitivity Analysis and Particle Swarm Optimization

Yufei Tang, Ping Ju, *Senior Member, IEEE*, Haibo He, *Senior Member, IEEE*, Chuan Qin, and Feng Wu

Abstract—Optimal control of large-scale wind farm has become a critical issue for the development of renewable energy systems and their integration into the power grid to provide reliable, secure, and efficient electricity. Among many enabling technologies, the latest research results from both the power and energy community and computational intelligence (CI) community have demonstrated that CI research could provide key technical innovations into this challenging problem. In this paper, we propose a sensitivity analysis approach based on both trajectory and frequency domain information integrated with evolutionary algorithm to achieve the optimal control of doubly-fed induction generators (DFIG) based wind generation. Instead of optimizing all the control parameters, our key idea is to use the sensitivity analysis to first identify the critical parameters, the unified dominate control parameters (UDCP), to reduce the optimization complexity. Based on such selected parameters, we then use particle swarm optimization (PSO) to find the optimal values to achieve the control objective. Simulation analysis and comparative studies demonstrate the effectiveness of our approach.

Index Terms—Computational intelligence, DFIG, optimized control, particle swarm optimization, sensitivity analysis, smart grid.

I. INTRODUCTION

WITH THE continuous increase of energy demand and environment concerns, the development of a smart electric power grid has become a critical research topic world widely [1], [2]. To tackle the critical challenges and develop a truly smart grid, extensive efforts have been devoted into this area at different levels, ranging from academic research, industrial research and development (R&D), to government policy makers [1]–[4]. While the entire smart grid system is an extremely complicated integrative technology and social system, in this paper we focus on one of the critical components to the whole picture, optimal control of wind turbine (WT) with doubly-fed induction generators (DFIG) based on sensitivity analysis and particle swarm optimization (PSO).

H. He and Y. Tang are with the Department of Electrical, Computer and Biomedical Engineering, University of Rhode Island, Kingston, RI 02881, USA (e-mail: he@ele.uri.edu; ytang@ele.uri.edu).

P. Ju, C. Qin and F. Wu are with the Hohai University, Nanjing, China (e-mail: pju@hhu.edu.cn; cqin@hhu.edu.cn; wufeng@hhu.edu.cn)

DFIG is widely used in the wind power system for its advantages over other wind turbine generators, such as squirrel-cage induction generator and permanent magnet synchronous generator [5]. The characteristics of DFIG are high efficiency, flexible control and low investment. The stator of DFIG is directly connected to the power grid while the rotor is connected to the power grid through a back-to-back converter, which only takes about 20%–30% of the DFIG rated capacity for the reason that the converter only supplies the exciting current of the DFIG. The back-to-back converter consists of three part: rotor side converter (RSC), grid side converter (GSC), and dc link capacitor. The controllers of the converter have significant effect on the stability of grid-connected DFIG [6].

In previous research, the stability analysis and optimal control of WT with DFIG had been studied by many researchers [7], [8], [25], [26], [28]–[30]. One of the key challenges for DFIG based wind farm optimization is the involvement of a large number of parameters need to be optimized to ensure a good interaction of the wind power with the power grid at the common coupling point (CCP). For instance, in [7], the authors presented an approach to use PSO to optimize all the control parameters in a DFIG simultaneously. This method can improve the performance of the DFIG in the power grid, however, when the number of the DFIG in a wind farm increases, the number of the control parameters will increase significantly. Therefore, advanced coordinated control approaches such as adaptive dynamic programming (ADP) based methods have showed great success and promising for such a challenging problem [9]–[12].

Sensitivity analysis has widely applications in power system analysis and modeling [13]–[16]. Eigenvalue sensitivity analysis [17] and voltage sensitivity analysis [19] based on DFIG system was also investigated by other researchers. In [17], the author applied eigenvalue sensitivity analysis on a DFIG system and found that the impact of different DFIG parameters on different critical eigenvalue pairs at different rotor speeds was different. One of the key questions for this is how to identify a uniformed dominate control parameters (UDCP) which can be used in the control optimization and reduce the optimization complexity for large-scale wind farms.

In this work, we propose a sensitivity analysis based optimal control of WT with DFIG using the PSO technique motivated from our previous work [7]. Through sensitivity analysis with both trajectory sensitivity analysis and eigenvalue sensitivity analysis, the UDCP can be obtained. Then we propose to use PSO to optimize these UDCP to improve the dynamic performance of the wind generation system. Simulation studies are
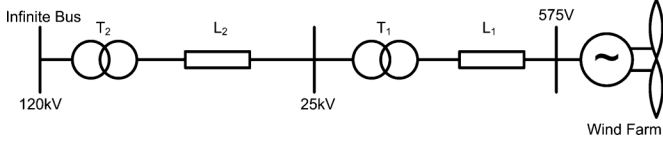
Fig. 1. Single-line diagram of the benchmark power system that includes a DFIG-based wind farm.
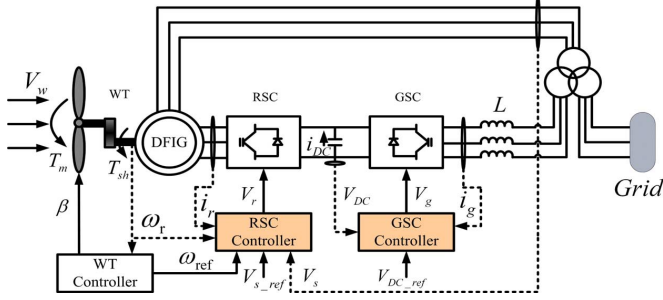

Fig. 2. Schematic diagram of DFIG wind turbine system [17], [18].

carried out in MATLAB/SIMULINK to verify the effectiveness of proposed method.

II. POWER SYSTEM MODEL

Normally, there are tens to hundreds wind turbines in a large wind farm. From previous research, if the controller of the wind turbines are well-tuned, there will be no mutual interaction between wind turbines on a wind farm [20]. Therefore, in this paper, the wind farm will be represented by one WT with DFIG system. Fig. 1 shows the diagram of the simulated single wind farm infinite bus system in MATLAB/SIMULINK. A 36 MW wind farm consisting of twenty-four 1.5 MW wind turbines connected to a 25 kV distribution system exports power to a 120 kV grid through a 30 km, 25 kV feeder. This 120 kV grid represents an infinite bus to the wind farm. Wind turbines use a DFIG consisting of a wound rotor induction generator and an ac/dc/ac insulated-gate bipolar transistor (IGBT) based pulse width modulation (PWM) converters. The stator winding is connected directly to the 60 Hz grid while the rotor is fed at variable frequency through the ac/dc/ac converter. The detailed model of the DFIG wind turbine system is introduced in this paper.

III. DFIG WIND TURBINE SYSTEM MODEL

The wind turbine model studied in this paper is illustrated in Fig. 2 [17], [18]. In this system, the wind turbine is connected to the DFIG through a drive train system, which consist of a low and a high speed shaft with a gearbox in between. The DFIG system is an induction type generator in which the stator windings are directly connected to the three-phase grid and the rotor windings are fed through three-phase back-to-back IGBT based PWM converters. The back-to-back PWM converter consist of three parts: a rotor side converter (RSC), a grid side converter (GSC) and a dc link capacitor placed between the two converters. There controller also consist of three parts: rotor side controller, grid side controller and wind turbine controller. The function of these controllers are to produce smooth electrical power with constant voltage and frequency to the power grid whenever the wind system is working at sub-synchronous speed

or super-synchronous speed, depending on the velocity of the wind. Vector control strategy is employed for both the RSC and GSC to achieve decoupled control of active and reactive power.

A. Model of Generator

As DFIG is an induction machine, the $d - q - 0$ reference frame based model of DFIG can be represented as follows [7]:

$$\frac{X'_s}{\omega_s}\frac{di_{ds}}{dt} = v_{ds} - \left[R_s + \frac{(X_s - X'_s)}{\omega_s T'_0}\right] * i_{ds}$$
$$- (1 - s_r)E'_d - \frac{L_m}{L_{rr}}v_{dr}$$
$$\times -\frac{1}{\omega_s T'_0}E'_q - X'_s i_{qs} \qquad (1)$$

$$\frac{X'_s}{\omega_s}\frac{di_{qs}}{dt} = v_{qs} - \left[R_s + \frac{(X_s - X'_s)}{\omega_s T'_0}\right] * i_{qs}$$
$$- (1 - s_r)E'_q - \frac{L_m}{L_{rr}}v_{qr}$$
$$\times -\frac{1}{\omega_s T'_0}E'_d - X'_s i_{ds} \qquad (2)$$

$$\frac{dE'_d}{dt} = s_r\omega_s E'_q - \omega_s \frac{L_m}{L_{rr}}v_{qr}$$
$$- \frac{1}{T'_0} \times [E'_d + (X_s - X'_s)i_{qs}] \qquad (3)$$

$$\frac{dE'_q}{dt} = s_r\omega_s E'_d - \omega_s \frac{L_m}{L_{rr}}v_{dr}$$
$$- \frac{1}{T'_0} \times [E'_q + (X_s - X'_s)i_{ds}] \qquad (4)$$

where $E'_d = -(\omega_s * L_m/L_{rr} * \psi_{qr})$, $E'_q = -(\omega_s * L_m/L_{rr} * \psi_{dr})$, $X_s = \omega_s * L_{ss}$, $X'_s = \omega_s * [L_{ss} - (L_m^2/L_{rr})]$ and $T'_0 = L_{rr}/R_r$.

The parameters used in above equations are defined as follows:

ψ_{dr}	the d axis rotor flux linkages;
ψ_{qr}	the q axis rotor flux linkages;
L_{ss}	the stator self-inductance;
L_{rr}	the rotor self-inductance;
L_m	the mutual inductance;
R_r	the rotor resistance;
ω_s	the synchronous angle speed;
s_r	the rotor slip;
X_s	the stator reactance;
X'_s	the stator transient reactance;
E'_d	the d axis voltage behind the transient reactance;
E'_q	the q axis voltage behind the transient reactance;
T'_0	the rotor circuit time constant;
i_{ds}	the d axis stator current;

i_{qs}	the q axis stator current;
v_{ds}	the d axis stator terminal voltages;
v_{qs}	the q axis stator terminal voltages;
v_{dr}	the d axis rotor terminal voltages;
v_{qr}	the q axis rotor terminal voltages.

B. Model of Drive Train

The drive train system consist of turbine, a low and a high speed shaft, and a gearbox. This system can be represented by a two-mass model as follows:

$$2H_t \frac{d\omega}{dt} = T_m - T_{sh} \tag{5}$$

$$\frac{d\theta_{tw}}{dt} = \omega_t - \omega_r = \omega_t - (1 - s_r)\omega_s \tag{6}$$

$$2H_g \frac{ds_r}{dt} = -T_{em} - T_{sh} \tag{7}$$

$$T_{sh} = K_{sh}\theta_{tw} + D_{sh}\frac{d\theta_{tw}}{dt} \tag{8}$$

where

H_t	the inertia constants of the turbine;
H_g	the inertia constants of the generator;
ω_t	the WT angle speed;
ω_r	the generator rotor angle speed;
$\theta_{t\omega}$	the shaft twist angle;
K_{sh}	the shaft stiffness coefficient;
D_{sh}	the damping coefficient;
T_{sh}	the shaft torque;
T_m	the wind torque;
T_{em}	the electromagnetic torque.

T_m and T_{em} are given by:

$$T_m = \frac{0.5\rho\pi R^2 C_p V_w^3}{\omega_t} \tag{9}$$

$$T_{em} = \frac{P_s}{\omega_s} \tag{10}$$

where

$$C_p = \frac{1}{2}\left(\frac{RC_f}{\lambda} - 0.022\beta - 2\right)e^{-0.225RC_f/\lambda}. \tag{11}$$

The parameters used in above equations are defined as follows:

ρ	the air density;
R	the WT blade radius;
V_w	the wind speed;
C_f	the blade design constant coefficient;
β	the blade pitch angle;
λ	the blade tip speed ratio;

ω_s	the synchronous angle speed;
C_p	the power coefficient;
P_s	the stator active power.

C. Model of DC Link Capacitor

From Fig. 2, the active power flow through the back-to-back PWM converter is balanced by the dc link capacitor. The power balance equation can be represented as follow:

$$P_r = P_g + P_{DC} \tag{12}$$

where

P_r	the active power at the ac terminal of the RSC;
P_g	the active power at the ac terminal of the GSC;
P_{DC}	the active power of the dc link capacitor.

These are given by following equations:

$$P_r = v_{dr}i_{dr} + v_{qr}i_{qr} \tag{13}$$

$$P_g = v_{dg}i_{dg} + v_{qg}i_{qg} \tag{14}$$

$$P_{DC} = v_{DC}i_{DC} = -Cv_{DC}\frac{dv_{DC}}{dt} \tag{15}$$

where

i_{dr}	the d axis rotor currents;
i_{qr}	the q axis rotor currents;
i_{dg}	the d axis currents of the GSC;
i_{qg}	the q axis currents of the GSC;
v_{dr}	the d axis rotor voltage;
v_{qr}	the q axis rotor voltage;
v_{dg}	the d axis voltage of the GSC;
v_{qg}	the q axis voltage of the GSC;
v_{DC}	the dc link capacitor voltage;
i_{DC}	the current of the dc link capacitor;
C	the capacitance of the dc link capacitor.

Substituting (13)–(15) into (12), the model of the dc link capacitor can be derived as follows:

$$Cv_{DC}\frac{dv_{DC}}{dt} = v_{dg}i_{dg} + v_{qg}i_{qg} - (v_{dr}i_{dr} + v_{qr}i_{qr}). \tag{16}$$

D. Model of Rotor Side Controller

As we mentioned in Section III, the vector control strategy is used for the active power and reactive power control of WT with DFIG system. For the RSC controller, the active power and voltage are controlled independently via v_{qr} and v_{dr}, respectively. The control scheme is shown in Fig. 3, while control equations can be expressed as follows:
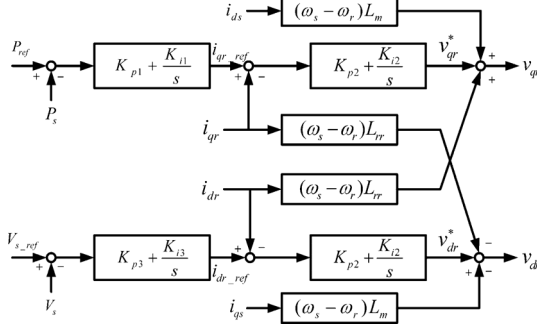
$$\frac{dx_1}{dt} = P_{ref} + P_s \tag{17}$$

Fig. 3. Schematic diagram of rotor side controller.

$$i_{qr\_ref} = K_{p1}(P_{ref} + P_s) + K_{i1}x_1 \tag{18}$$

$$\frac{dx_2}{dt} = i_{qr\_ref} - i_{qr} = K_{p1}(P_{ref} + P_s)$$
$$+ K_{i1}x_1 - i_{qr} \tag{19}$$

$$\frac{dx_3}{dt} = v_{s\_ref} - v_s \tag{20}$$

$$i_{dr\_ref} = K_{p3}(v_{s\_ref} - v_s) + K_{i3}x_3 \tag{21}$$

$$\frac{dx_4}{dt} = i_{dr\_ref} - i_{dr} = K_{p3}(v_{s\_ref} - v_s)$$
$$+ K_{i3}x_3 - i_{dr} \tag{22}$$

$$v_{qr} = K_{p2}(K_{p1}\Delta P + K_{i1}x_1 - i_{qr}) + K_{i2}x_2$$
$$+ s_r\omega_s L_m i_{ds} + s_r\omega_s L_{rr}i_{qr} \tag{23}$$

$$v_{dr} = K_{p2}(K_{p3}\Delta v + K_{i3}x_3 - i_{dr}) + K_{i2}x_4$$
$$- s_r\omega_s L_m i_{qs} - s_r\omega_s L_{rr}i_{dr} \tag{24}$$

where

$K_{p1}\&K_{i1}$	the PI gains of the power regulator;
$K_{p2}\&K_{i2}$	the PI gains of RSC Current regulator;
$K_{p3}\&K_{i3}$	the PI gains of the grid voltage regulator;
i_{dr_ef}	the current control references for the d axis components of the GSC;
i_{qr_ef}	the current control references for the q axis components of the GSC;
v_{s_ef}	the specified terminal voltage reference;
$0P_{ref}$	the active power control reference.

E. Model of Grid Side Controller

The GSC controller, as shown in Fig. 4, aims to maintain the dc link voltage and control the terminal reactive power. The dc link voltage and reactive power are controlled independently via i_{dg} and i_{qg}, respectively. The equations are given as follows:

$$\frac{dx_5}{dt} = v_{DC\_ref} - v_{DC} \tag{25}$$

$$i_{dg\_ref} = -K_{pdg}\Delta v_{DC} + K_{idg}x_5 \tag{26}$$

$$\frac{dx_6}{dt} = i_{dg\_ref} - i_{dg}$$
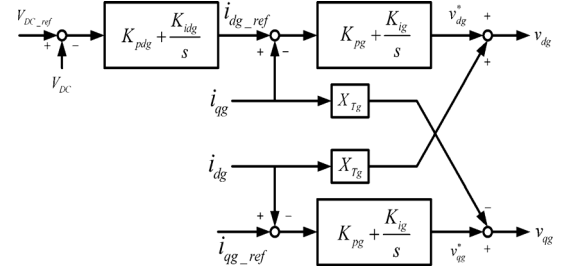$$= -K_{pdg}\Delta v_{DC} + K_{idg}x_5 - i_{dg} \tag{27}$$
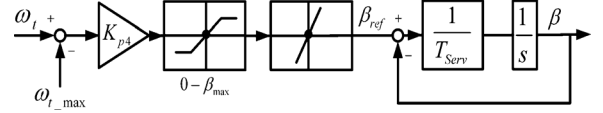

Fig. 4. Schematic diagram of grid side controller.

Fig. 5. Schematic diagram of pitch control.

$$\frac{dx_7}{dt} = v_{qg\_ref} - i_{qg} \tag{28}$$

$$\Delta v_{dg} = K_{pg}\frac{dx_6}{dt} + K_{ig}x_6$$
$$= K_{pg}(-K_{pdg}\Delta v_{DC} + K_{idg}x_5 - i_{dg})$$
$$+ K_{ig}x_6 \tag{29}$$

$$\Delta v_{qg} = K_{pg}\frac{dx_7}{dt} + K_{ig}x_7$$
$$= K_{pg}(i_{qg\_ref} - i_{qg}) + K_{ig}x_6 \tag{30}$$

where

$K_{pdg}\&K_{idg}$	the PI gains of the dc link capacitor voltage regulator;
$K_{pg}\&K_{ig}$	the PI gains of the grid side converter current regulator;
v_{DC_ef}	the voltage control reference of the dc link capacitor;
i_{qg_ef}	the control reference for the q axis component of the GSC current.

F. Model of Pitch Controller

The aim of pitch angle control is to optimize the power extraction of wind turbines as well as to prevent overrated power production in strong wind. The control scheme is illustrated in Fig. 5 with the following control equation:

$$\frac{d\beta}{dt} = K_{p4} - \frac{T_m - T_{sh}}{2H_t} + K_{i4}\Delta\omega_t \tag{31}$$

where K_{p4} and K_{i4} are the PI gains of the WT speed regulator, $\Delta\omega_t$ is the deviation of the WT rotating speed. The electrical dynamics are much faster than the mechanical dynamics, meaning the control of electrical dynamics can be decoupled from that of mechanical dynamics. The controllers of electrical dynamics are optimized while the parameters K_{p4} and K_{i4} are not included in the optimization. In this paper, we set $K_{p4} = K_{p2}$ and $K_{i4} = K_{i2}$.

From the discussions above, the model of WT with DFIG system can be represented in a compact form as follows:

$$\dot{X} = f(X, U) \tag{32}$$

where X and U are the vectors of the DFIG state variables and input variables defined as follows, respectively.

$$X = [\omega_t, \beta, \theta_{t\omega}, S_r, i_{ds}, i_{qs}, E'_d, E'_q, x_1, x_2, x_3, x_4, V_{DC}, x_5, x_6, x_7]^T \tag{33}$$

$$U = [v_{ds}, v_{qs}, i_{dg}, i_{qg}]^T. \tag{34}$$

IV. SENSITIVITY ANALYSIS

A. Trajectory Sensitivity Analysis

The trajectory sensitivity analysis investigates the degree of change of the system when a parameter of the system subjects to small changes. It reflects the derivative relations between the system trajectory and the system parameters. This method could significantly reduce the complexity of simulation and calculation. It has widely applications in the power system for parameters effects on the system dynamic performance, the effect of parameters uncertainty, parameters estimation, boundary problems, optimal control and stability assessment. In this paper, the numerical difference method is employed to calculate the trajectory sensitivity of the DFIG control parameters [21].

The analytical description of a power system applicable to trajectory sensitivity analysis is given by the following differential-algebraic equation (DAE):

$$\begin{cases} \frac{dx}{dt} = f(x, y, \theta) \\ 0 = g(x, y, \theta) \\ x(t_0) = x_0 \\ y(t_0) = y_0 \end{cases} \tag{35}$$

where x correspond to the system state variables and y represent system output variables. θ is the control parameters. The sensitivity of the control parameters are evaluated along the trajectory. The numerical procedure to evaluate these sensitivities using data from time domain simulations can be represented by the following equations:

$$\frac{\partial y_i(\theta, k)}{\partial \theta_j}$$
$$= \lim_{\Delta\theta_j \to 0} \frac{y_i(\theta_1, \ldots, \theta_j + \Delta\theta_j, \ldots, \theta_m, k) - y_i(\theta_1, \ldots, \theta_j, \ldots, \theta_m, k)}{\Delta\theta_j} \tag{36}$$

where y_i represents the trajectory curve of the ith variable and corresponds to the jth control parameter. m is the total number of control parameters, k is the time instance, and $\Delta\theta_j$ is the change of the parameter of θ. Using the median method to calculate the derivative to avoid the deflection error and improve the accuracy of the numerical calculation, we need to calculate

the system trajectory twice, either by increment or decrement of a $\Delta\theta_j$:

$$\begin{cases} y_i(\theta_1, \ldots, \theta_j + \Delta\theta_j, \ldots, \theta_m, k) \\ y_i(\theta_1, \ldots, \theta_j - \Delta\theta_j, \ldots, \theta_m, k). \end{cases} \tag{37}$$

Then the relative value of the trajectory sensitivity can be calculated as:

$$\frac{\partial\left[\frac{y_i(\theta, k)}{y_{i0}}\right]}{\partial\left[\frac{\theta_j}{\theta_{j0}}\right]}$$
$$= \frac{\frac{[y_i(\theta_1, \ldots, \theta_j + \Delta\theta_j, \ldots, \theta_m, k) - y_i(\theta_1, \ldots, \theta_j - \Delta\theta_j, \ldots, \theta_m, k)]}{y_{i0}}}{\frac{2\Delta\theta_j}{\theta_{j0}}} \tag{38}$$

where θ_{j0} is the given value of parameter θ_j and y_{j0} is the corresponding steady-state value given θ_{j0}.

Using the equation above, we can obtain a group of trajectory sensitivity. To compare the sensitivity value of these different control parameters, we can calculate the mean trajectory sensitivity as follows:

$$A_{ij} = \frac{1}{K} \sum_{k=1}^{K} \left| \frac{\partial\left[\frac{y_i(\theta, k)}{y_{i0}}\right]}{\partial\left[\frac{\theta_j}{\theta_{j0}}\right]} \right| \tag{39}$$

where K is the sampling number on the trajectory sensitivity curves.

If the sensitivity of trajectory y_i to the control parameter θ_j is large, then the trajectory sensitivity of this control parameter is large likewise. It represents that the control parameter θ_j has large influence on the system trajectory y_i. We call these control parameters as dominate control parameters. On the contrary, if the control parameter θ_j barely has influence on the system trajectory, then the trajectory sensitivity of these control parameters will be small.

B. Eigenvalue Sensitivity Analysis

Linearize the DAE in (35) at the operating point, the power system state equation can be obtained:

$$\dot{X} = AX \tag{40}$$

where A is the Jacobian matrix of the system. Then the characteristic equation of the system is:

$$|\lambda I - A| = 0 \tag{41}$$

where I is a unit matrix which has the same dimension as A. Through (41), we could obtain the system eigenvalue $\lambda_1, \lambda_2, \ldots, \lambda_n$[13].

The Jacobian matrix A is a function of the control parameter θ which can be written as $A(\theta)$. Then any of the system eigenvalue $\lambda_1, \lambda_2, \ldots, \lambda_n$ of $A(\theta)$ will be the function of θ, similarly could be written as $\lambda_i(\theta)$. When the control parameter changes, the $\lambda_i(\theta)$ will change correspondingly, which will reflect the influence of control parameters θ on the system stability.
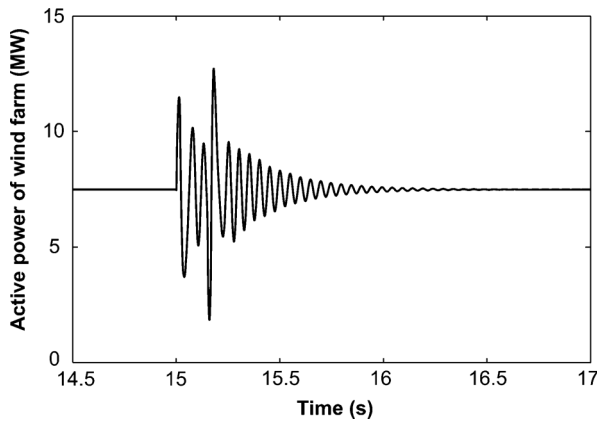
Fig. 6.   Active power of WT with DFIG.

The sensitivity of eigenvalue λ_i to control parameter θ is calculated as follows:

$$\frac{\partial \lambda_i(\theta)}{\partial \theta_j} = v_i^T \frac{\partial A(\theta)}{\partial \theta_j} u_j \tag{42}$$

where v and u are right and left eigenvector, respectively. This equation is a complex number which can reflect the influence of small change of system control parameter on system eigenvalue λ_i, where the modulus and phase represent the moving direction and size, respectively. These eigenvalue sensitivities are useful for the selection of dominate control parameters and will be described later.

V. DFIG CONTROL PARAMETERS SENSITIVITY ANALYSIS

A. DFIG Control Parameters Trajectory Sensitivity Analysis

The configuration of the simulation system is in Fig. 1. The fault is located at the Bus-25 KV. The fault type is set to three-phase ground fault starts at 15 s and last for 0.15 s. The fault resistance of each phase is $20 \ \Omega$. The active power trajectory of the DFIG is chosen as the object function in our current study. Fig. 6 shows the active power of DFIG under the fault condition. It can be seen that the active power will become stable at about 16.5 s. The sampling interval is from 15.15 s to 16.5 s and the sampling time is 0.001 s. The total number of points for trajectory sensitivity analysis is 1350.

The procedure of trajectory sensitivity analysis is as follows:
  1) From Section III, we have a total of ten control parameters for the controller of the Wind Turbine system: K_{p1}, K_{i1}, K_{p2}, K_{i2}, K_{p3}, K_{i3}, K_{pdg}, K_{idg}, K_{pg} and K_{ig}. Increase the value of these control parameters 10%, and obtain the trajectory of DFIG active power.
  2) Decrease the value of these ten control parameters by 10%, and obtain the trajectory of DFIG active power as in step 1).
  3) According to equation (39), computing the trajectory sensitivity of each control parameter.

Table I shows the sensitivities of each control parameters, and Table II shows the group of these parameters according to their values.

It can be seen that K_{i3} is the largest one with trajectory sensitivity value of 2.2838 and K_{pg} is the smallest one with a value

TABLE I
SENSITIVITY OF EACH CONTROL PARAMETERS

Parameter	Sensitivity value
K_{p1}	1.1251
K_{i1}	0.1100
K_{p2}	0.6093
K_{i2}	0.0949
K_{p3}	0.5755
K_{i3}	2.2838
K_{pdg}	0.0421
K_{idg}	0.0072
K_{pg}	0.0010
K_{ig}	0.0311

TABLE II
CLASSIFY THE SENSITIVITY OF CONTROL PARAMETERS

Order	Parameters
The first order	K_{i3}, K_{p1}
The second order	K_{i1}, K_{p2}, K_{i2}, K_{p3}
The third order	K_{pdg}, K_{idg}, K_{pg}, K_{ig}

TABLE III
SYSTEM EIGENVALUE AND PARTICIPATION FACTORS ANALYSIS

λ	σ	ω	f	ASV_1	ASV_2
λ_1	-12612	0	0	V_{DC}	$-$
λ_2	-174.8	0	0	x_5	x_6
$\lambda_{3,4}$	-69.5	112.9	18	E_q'	x_3
$\lambda_{5,6}$	-94.1	44.6	7.1	E_d'	x_1
$\lambda_{7,8}$	-2.24	60	9.6	θ_{tw}	S_r
λ_9	-75.9	0	0	E_d'	x_1
$\lambda_{10,11}$	-0.5	0.77	0.12	ω_t	β
λ_{12}	-14.5	0	0	x_5	x_6
λ_{13}	-25.1	0	0	x_4	$-$
λ_{14}	-24.1	0	0	x_2	$-$

of 0.001. Therefore, we choose K_{i3} and K_{p1} as the dominate control parameters for the trajectory sensitivity analysis.

B. DFIG Control Parameters Eigenvalue Sensitivity Analysis

From Section III, we have the system state vector as follows:

$$X = \left[\omega_t, \beta, \theta_{tw}, S_r, i_{ds}, i_{qs}, E_d', E_q', x_1, x_2, x_3, x_4, V_{DC}, x_5, x_6, x_7\right]^T. \tag{43}$$

In this paper, the stator transients may be neglected in the small signal stability analysis. Then state vector became:

$$X = \left[\omega_t, \beta, \theta_{tw}, S_r, E_d', E_q', x_1, x_2, x_3, x_4, V_{DC}, x_5, x_6, x_7\right]^T. \tag{44}$$

Then through small signal stability analysis, we could get the system eigenvalue and participation factors, as shown in Table III.

The system is stable since all the eigenvalues have negative real parts. In particular, there are four modes of oscillation: one is associated with E_q' and x_3 with the frequency of 18 Hz, one is associated with E_d' and x_1 with the frequency of 7.1 Hz, one is associated with θ_{tw} and S_r with the frequency of 9.6 Hz, and the last one is associated with ω_t and β with the frequency of 0.12 Hz.

TABLE IV
EIGENVALUE SENSITIVITIES OF CONTROL PARAMETERS TO EACH EIGENVALUE

λ	K_{p1}	K_{i1}	K_{p2}	K_{i2}	K_{p3}	K_{i3}	K_{pdg}	K_{idg}	K_{pg}	K_{ig}
λ_1	0.8607	0.0214	7.7291	0.1924	0.3387	0.0084	35.5997	0.0071	13.5367	1.2347
λ_2	0.0057	0.0102	0.0473	0.0849	0.0007	0.0013	0.2319	0.5562	0.3052	1.9171
$\lambda_{3,4}$	0.0286	0.0678	1.1115	2.6322	0.0729	0.1726	$6.9e^{-5}$	0.0001	0.0379	0.0899
$\lambda_{5,6}$	0.1566	0.4721	0.8931	2.691	0.0310	0.0936	0.0003	0.0019	0.1463	0.4431
$\lambda_{7,8}$	$7.9e^{-4}$	0.0042	0.0069	0.0359	$5.9e^{-6}$	$3.1e^{-5}$	$7.9e^{-8}$	$3.6e^{-7}$	$1.5e^{-5}$	$7.8e^{-5}$
λ_9	0.1318	0.5450	0.4276	1.771	0.0032	0.0134	$6.3e^{-6}$	0.0001	0.04295	0.1776
$\lambda_{10,11}$	$3.8e^{-9}$	$1.3e^{-6}$	$3.6e^{-8}$	$1.2e^{-5}$	$6e^{-14}$	$2e^{-11}$	$1e^{-14}$	$3e^{-12}$	$5e^{-12}$	$1e^{-9}$
λ_{12}	$4.4e^{-8}$	$9.7e^{-7}$	$3.5e^{-7}$	$7.7e^{-6}$	$5.8e^{-10}$	$1.2e^{-8}$	0.0217	0.5510	0.0212	0.0133
λ_{13}	$3.8e^{-4}$	0.0049	0.2171	2.7153	0.0006	0.0077	$6.8e^{-8}$	$1.1e^{-6}$	$7.8e^{-5}$	0.0010
λ_{14}	0.0034	0.0444	0.1856	2.4162	0.0002	0.0020	$1.5e^{-6}$	$2.6e^{-5}$	0.0001	0.0016

TABLE V
CLASSIFY THE SENSITIVITY OF CONTROL PARAMETERS

λ	Control parameters array by eigenvalue sensitivity
λ_1	$K_{pdg} > K_{pg} > K_{p2} > K_{ig} > K_{p1} > K_{p3} > K_{i2} > K_{i1} > K_{i3} > K_{idg}$
λ_2	$K_{ig} > K_{idg} > K_{pg} > K_{pdg} > K_{i2} > K_{p1} > K_{p2} > K_{i1} > K_{i3} > K_{p3}$
$\lambda_{3,4}$	$K_{i2} > K_{p2} > K_{i1} > K_{ig} > K_{p3} > K_{pg} > K_{p1} > K_{i3} > K_{idg} > K_{pdg}$
$\lambda_{5,6}$	$K_{i2} > K_{p2} > K_{i1} > K_{ig} > K_{p1} > K_{pg} > K_{i3} > K_{p3} > K_{idg} > K_{pdg}$
$\lambda_{7,8}$	$K_{i2} > K_{p2} > K_{i1} > K_{p1} > K_{ig} > K_{p3} > K_{pg} > K_{i3} > K_{idg} > K_{pdg}$
λ_9	$K_{i2} > K_{i1} > K_{p2} > K_{ig} > K_{p1} > K_{pg} > K_{i3} > K_{p3} > K_{idg} > K_{pdg}$
$\lambda_{10,11}$	$K_{i2} > K_{i1} > K_{p2} > K_{p1} > K_{ig} > K_{i3} > K_{pg} > K_{idg} > K_{p3} > K_{pdg}$
λ_{12}	$K_{idg} > K_{pdg} > K_{pg} > K_{ig} > K_{i2} > K_{i1} > K_{p2} > K_{p1} > K_{i3} > K_{p3}$
λ_{13}	$K_{i2} > K_{p2} > K_{i3} > K_{i1} > K_{ig} > K_{p3} > K_{p1} > K_{pg} > K_{idg} > K_{pdg}$
λ_{14}	$K_{i2} > K_{p2} > K_{i1} > K_{p1} > K_{i3} > K_{ig} > K_{p3} > K_{pg} > K_{idg} > K_{pdg}$

Using (42), the eigenvalue sensitivities of each control parameter can be obtained. Table IV shows the eigenvalue sensitivities of control parameters, and Table V shows a sorted array according to their values. From Tables IV and V, one can see the control parameter K_{pdg} has the largest eigenvalue sensitivity in response to λ_1 (with the value of 35.5997). The eigenvalue sensitivity of k_{pg} is also much bigger than others in response to λ_1 (with the value of 13.5367). Therefore, both K_{pdg} and k_{pg} are chosen to be the dominate control parameters. K_{i1} and K_{i2} are consider as a dominate control parameter as well, because for most of the eigenvalue ($\lambda_{3,4}$, $\lambda_{5,6}$, $\lambda_{7,8}$, λ_9, $\lambda_{10,11}$, λ_{13}, λ_{14}), K_{i1} and K_{i2} dominate eigenvalue sensitivity. Therefore, we choose K_{pdg}, K_{pg}, K_{i1} and K_{i2} as the dominate control parameters for the eigenvalue sensitivity analysis in our study.

From above discussion, we have K_{i3} and K_{p1} as the dominate control parameter for the trajectory sensitivity analysis and K_{pdg}, K_{pg}, K_{i1} and K_{i2} as the dominate control parameters for the eigenvalue sensitivity analysis. The unified dominate control parameters (UDCP) are: K_{p1}, K_{i1}, K_{i2}, K_{i3}, K_{pdg} and K_{pg}.

VI. UDCP OPTIMIZATION USING PSO

PSO was originally developed by Kennedy and Eberhart for simulating social behavior, as a stylized representation of the movement of organisms in a bird flock or fish school [22]. PSO is a metaheuristic algorithm which means that it makes few or no assumptions about the problem being optimized and can search very large spaces of candidate solutions. PSO can be used on optimization problems that are partially irregular, noisy, or change over time.

Since the model of WT with DFIG system is a high-dimensional multivariate time-varying system, we choose PSO to search the optimal parameters for the controller of the WT

system. For the purpose to verify our approach, we compare three optimization options in this work:

Option One: optimize all the ten control parameters: K_{p1}, K_{i1}, K_{p2}, K_{i2}, K_{p3}, K_{i3}, K_{pdg}, K_{idg}, K_{pg}, K_{ig} simultaneously.

Option Two: optimize the six UDCP: K_{p1}, K_{i1}, K_{i2}, K_{i3}, K_{pdg} and K_{pg}. The other four control parameters we set as default value.

Option Three: optimize random six control parameters.

The procedure of the optimization is design as follows:

Step One: Initialization

There are n (10 or 6 in this paper) control parameters for the controller of WT with DFIG. So n particle positions for each member in particle swarm $\{x_{i,j}(0), i = 1, 2, \ldots, \Delta j = 1, 2, \ldots, n\}$ can be generated randomly around the original values as follows.

$$x_i, j(0) = X_{i0} * \left[1 \pm \frac{5}{100} * rand(1, 1)\right] \quad (45)$$

where x_{i0} represents the original value or original position. Then the upper and lower bounds, X_{max} and X_{min} of the parameters should be specified to define the range of the searching space.

The velocity for the position updating should also be initialized.

$$v_{j,\max} = \frac{x_{j,\max} - x_{j,\min}}{N}$$
$$v_{j,\min} = -v_{j,\max}, \quad j = 1, 2, \ldots, n \quad (46)$$

where $x_{j,\max}$ and $x_{j,\min}$ are the upper and lower bounds of member j of particles, respectively, $v_{j,\max}$ and $v_{j,\min}$ are the maximum and minimum velocities of member j of particles, respectively, N is the interval of dimension, which is normally chosen between 5 and 10. Then the initial velocities $V(0) = \{v_{i,j}(0), i = 1, 2, \ldots, m, j = 1, 2, \ldots, n\}$ are generated randomly between $[v_{j,\min}, v_{j,\max}]$. The other parameters are initialized as follows:

$$\begin{cases} c_1 = 2, c_2 = 2 \\ \alpha = 0.98 \\ w_i = 0.9, w_f = 0.2 \\ Number of Particles : 100 \end{cases} \quad (47)$$

where c_1 and c_2 are the accelerating constants. α is the decay constant. w_i and w_f are the initial and final weights.

TABLE VI
CONTROL PARAMETERS WITH AND WITHOUT OPTIMIZATION

Options	K_{p1}	K_{i1}	K_{p2}	K_{i2}	K_{p3}	K_{i3}	K_{pdg}	K_{idg}	K_{pg}	K_{ig}
Oroginal	1	100	0.3	8	1.25	300	0.002	0.05	1	100
OptionOne	1.2062	80.3710	0.2719	5.0946	1.4804	219.1246	0.0119	0.0539	0.7338	130.8737
OptionTwo	1.2068	79.3829	0.3	5.1028	1.25	221.5749	0.012	0.05	0.7401	100
OptionThree	1.0121	100	0.3	8	1.2095	327.8310	0.002	0.0524	0.8119	97.8897

TABLE VII
EIGENVALUE ANALYSIS WITH OPTION ONE

λ	λ_1	λ_2	$\lambda_{3,4}$	$\lambda_{5,6}$	$\lambda_{7,8}$	λ_9	$\lambda_{10,11}$	λ_{12}	λ_{13}	λ_{14}
σ	−66937	−193	−95.62	−112.15	−2.44	−49.5	−0.51	−4.18	−17.3	−17.9
ω	0	0	79	55.5	60	0	0.77	0	0	0

TABLE VIII
EIGENVALUE ANALYSIS WITH OPTION TWO

λ	λ_1	λ_2	$\lambda_{3,4}$	$\lambda_{5,6}$	$\lambda_{7,8}$	λ_9	$\lambda_{10,11}$	λ_{12}	λ_{13}	λ_{14}
σ	−66583	−147.4	−100.32	−2.39	−94.8	−46.5	−0.51	−3.89	−16	−16.4
ω	0	0	100.34	60	42.8	0	0.77	0	0	0

TABLE IX
EIGENVALUE ANALYSIS WITH OPTION THREE

λ	λ_1	λ_2	$\lambda_{3,4}$	$\lambda_{5,6}$	$\lambda_{7,8}$	λ_9	$\lambda_{10,11}$	λ_{12}	λ_{13}	λ_{14}
σ	−11640	−191.8	−69	−100	−2.24	−77.4	−0.50	−24	−25	−16
ω	0	0	117.9	52.8	60	0	0.76	0	0	0

Step Two: Evaluating individual best solution and global best solution and updating

Evaluate the fitness value of the initial group of particles, which is given by

$$F = \max \{\mathrm{Real}(\lambda_l),\ l = 1, 2, \ldots, 14\} \quad (48)$$

where F is the fitness value, λ_l is the eigenvalue of the WT with DFIG system and l is the number of the state variables. The optimization objective is to minimizes F in order to drive all the eigenvalues as far to the left of the imaginary axis as possible. The individual best solution and global best solution to the problem will be determined on the fitness value. After each iteration, the individual best solution and global best solution should be updated.

Step Three: Velocities and positions updating

The velocity and position updating of PSO are conducted as follows.

$$v_{i,j}(t+1) = \omega(t) * v_{i,j}(t) + c_1 r_1(x^* - x_{i,j}(t))$$
$$+ c_2 r_2(x^{**} - x_{i,j}(t)) \quad (49)$$
$$x_{i,j}(t+1) = x_{i,j}(t) + v_{i,j}(t+1) \quad (50)$$

where r_1 and r_2 are uniformly distributed random numbers in $[0, 1]$, x^* and x^{**} are the individual and global best solution so far.

Step Four: Stopping criteria

If the stop conditions are satisfied, search process will be terminated. In this paper, the search will terminate if one of the following criteria is satisfied:

1) The time counter is greater than the maximal number specified;

2) The fitness value of global best solution is smaller than a specified number;

If one of the stopping criteria is satisfied, then stop; otherwise, the system will keep iterate until to step 2.

The PSO algorithm presented above is used to tune the parameters of the controller of the WT with DFIG system. The results of the three options is represented in Table VI. Based on the optimized control parameters in this table, small signal stability analysis is carried out, and the results are shown in the Tables VII–IX for options one, two, and three, respectively. It can be observed that optimizing the UDCP has the similar result as the optimize all the ten control parameters.

The computational complexity analysis is also carried out in this paper to compare the efficiency of option one and option two. It can be observed from Table X that the optimization time decrease from 58 ms to 35 ms with the proposed approach. The efficiency increase about 40%.

VII. COMPUTER SIMULATION STUDY

In previous sections, we derived the mathematical model of WT with DFIG system and present the approach by using PSO

TABLE X
COMPUTATION COMPLEXITY ANALYSIS

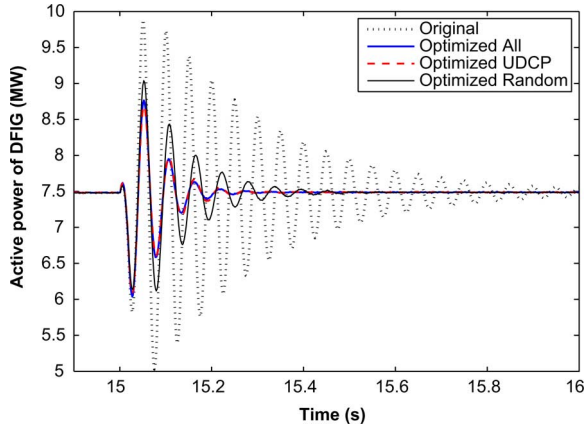| Number of control parameters	Each iteration time(ms)	Number of iteration	Total time(ms)
10	0.58	100	58
6	0.35	100	35

Fig. 7.   Active power of the WT with DFIG under small disturbance.

Fig. 8.   Reactive power of the WT with DFIG under small disturbance.

Fig. 9.   Voltage of dc link under small disturbance.

to find the optimized UDCP control parameters. In this section, we present the simulations in MATLAB/SIMULINK to verify the improvement in dynamic stability by the controller of the WT with DFIG system with the optimized UDCP control parameters. Both single machine infinite bus (SMIB) power system and multi-machine power system are investigated in our current study.

A. Case 1: SMIB Power System With Small Disturbance

The SMIB power system is illustrated in Fig. 1. The small disturbance is set as the DFIG voltage reference decrease from 1.0 pu to 0.9 pu. The dynamics of the output active power, output reactive power and dc link voltage are demonstrated in Figs. 7, 8 and 9, respectively. Each of these figures show four curves with different parameters: the original control parameters, optimized all ten control parameters, optimized random six control parameters and optimized UDCP. It can be observed that using the optimized UDCP, the dynamic performance of the WT with DFIG system is almost the same as using all the ten optimized control parameters. The magnitudes of the active power, reactive power and voltage sag and overshoot have been reduced significantly. The oscillation damped with the optimized UDCP is also much better than that without the optimization. Also, it can be observed that although the performance of optimized random six control parameters is better than the original one, it can not compete with our proposed approach with the optimized UDCP.

B. Case 2: SMIB Power System With Large Disturbance

A large disturbance is also applied on the simulation system. To do this, a three-phase ground fault is simulated in the middle of the transmission line. The fault is applied at the time $t = 15$, and cleared after 0.15 s. The dynamics of the output active power, output reactive power and dc link voltage are simulated. Figs. 10–12 are the simulation results of active power, reactive power, and voltage of dc link, respectively, with four choices of
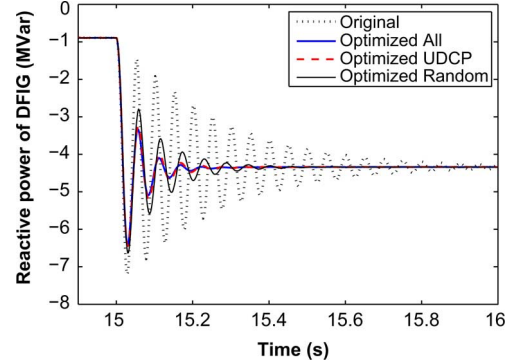
parameters: original control parameters, optimized all ten control parameters, optimized random six control parameters, and optimized UDCP. It can be observed that using the optimized UDCP, the dynamic performance of the WT with DFIG is almost the same as using all the ten optimized control parameters. The oscillation after the disturbance was damped out very quickly as similar as in the small disturbance in case 1. Therefore, the optimized UDCP enhances the fault ride-through capability of the WT system. Also, it can be observed that the performance of optimized random six control parameters is not as good as optimized UDCP. These results are consistent with our objective, namely, the sensitivity analysis based optimized control of the WT systems has good performance.

C. Case 3: Multi-Machine Power System

To test the robustness of the optimized control parameters, a multi-machine power system is also used in this paper. Fig. 13 is the revised four-machine-two-area system based on the classic model. This power system model first appeared in [24] to investigate the impact of the wind turbine with different controllers such as the optimized PI controller and nonlinear controller on the transient stability performance of the power system. The system is divided into two areas, in each of which there are two
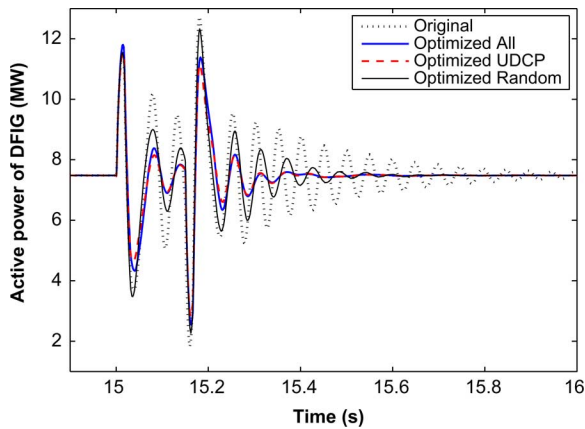
Fig. 10. Active power of the WT with DFIG under large disturbance.
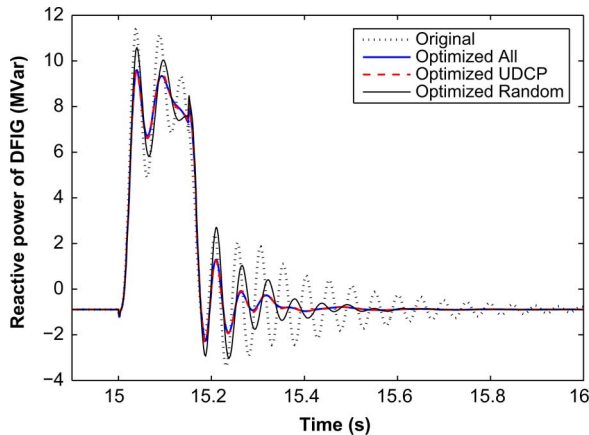

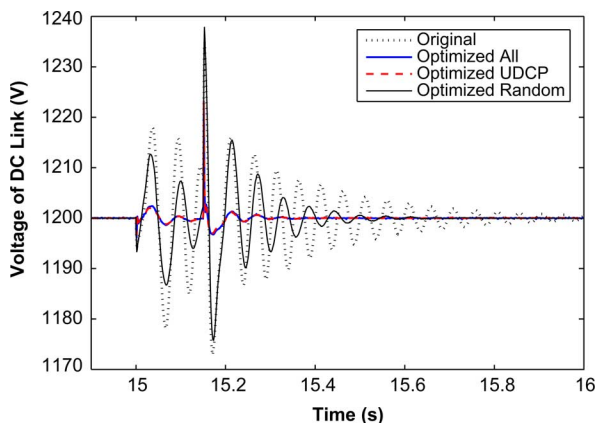Fig. 11. Reactive power of the WT with DFIG under large disturbance.

Fig. 12. Voltage of dc link under large disturbance.

machines. In [24], the four-machine-two-area system is modified by replacing generator G4 with a DFIG, which is the same as that used in the above SMIB power system. The DFIG capacity is 36 MW as indicated in Section II, where the other three synchronous machines have the same capacity as the DFIG. Before the fault occurs, the active power transfer from area one to area two is almost 15 MW. Power flow data and system parameters could refer to [24].

A single phase ground fault is applied in the middle of the transmission line 1. The fault is applied at the time $t = 30$, and cleared after 0.2 s without tripping the line. The dynamics of the output active power, voltage of the DFIG and dc link voltage are simulated. Figs. 14–16 are the simulation results of
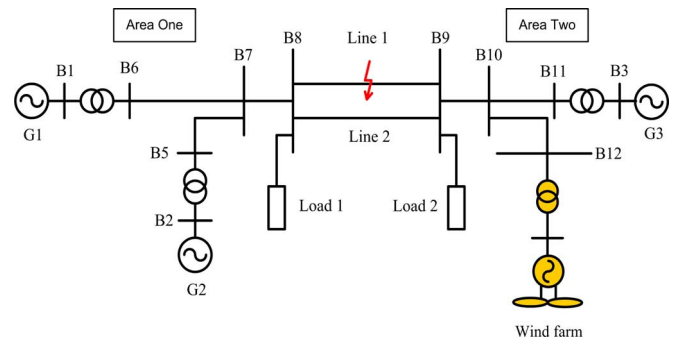

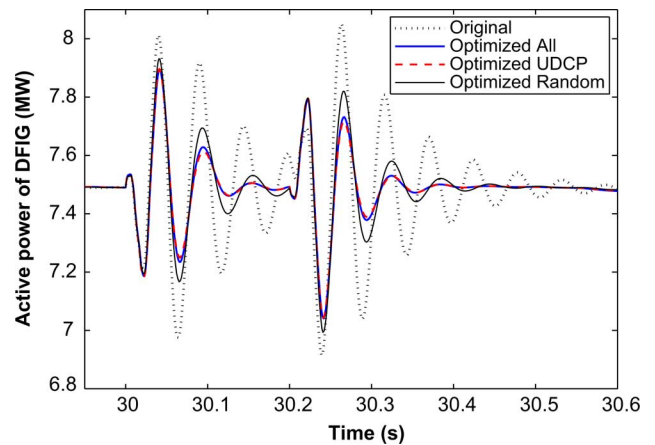Fig. 13. Schematic diagram of multi-machine power system with DFIG.

Fig. 14. Active power of the WT with DFIG in multi-machine power system.

active power, voltage of DFIG, and voltage of dc link, respectively, with four choices of parameters: original control parameters, optimized all ten control parameters, optimized random six control parameters and optimized UDCP. It can be observed that using the optimized UDCP, the dynamic performance of the WT with DFIG is almost the same as using all the ten optimized control parameters. Moreover, the performance of using UDCP is better than using the optimized random six control parameters. The oscillation after the disturbance was damped out very quickly as similar as in the SMIB power system. As generator 3 (G3) is near the DFIG, its dynamic responses will be affected significantly. The voltage of G3 is illustrated in Fig. 17. It can be observed that the oscillation of the voltage of G3 is damped quickly. Therefore, the optimized UDCP is also effective in the multi-machine power system.

VIII. CONCLUSIONS AND FUTURE WORK

In this paper, a detailed wind turbine system with DFIG model including induction generator, drive train, back-to-back PWM converters, pitch control, RSC, GSC, and their controllers were presented. Sensitivity analysis based on trajectory sensitivity analysis and eigenvalue sensitivity analysis was carried out on the DFIG control parameters. PSO algorithm was employed to find the optimal control parameters in order to achieve the optimal control of the multiple controllers of the wind turbine system. The small signal stability analysis of the wind turbine system with and without optimized control parameters was carried out. Simulation on MATLAB/SIMULINK
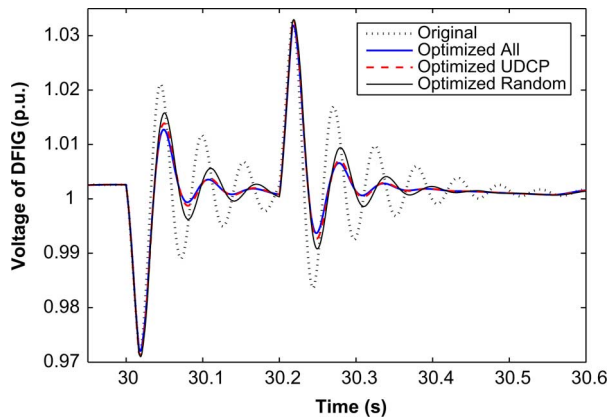
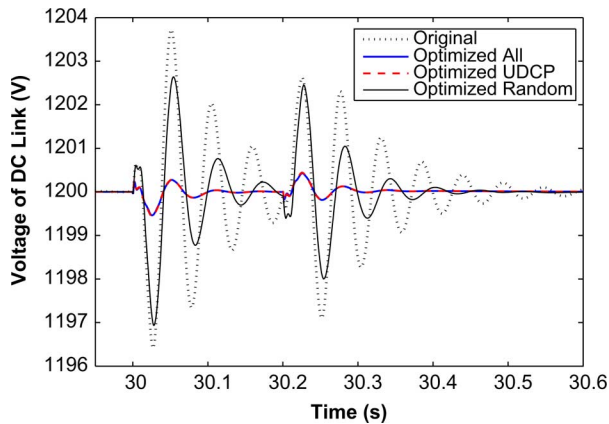Fig. 15.   Voltage of the WT with DFIG in multi-machine power system.

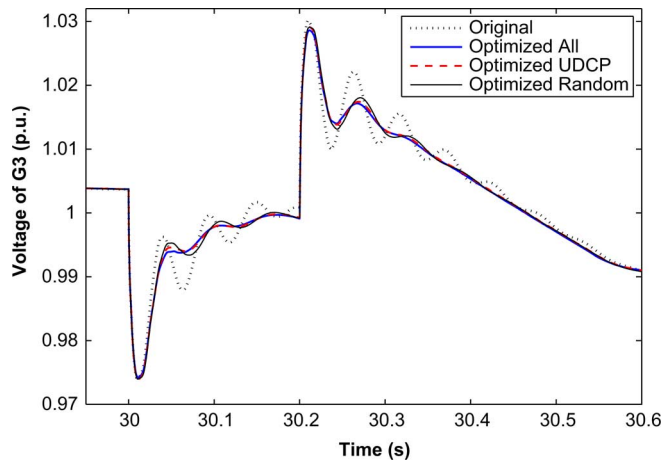Fig. 16.   Voltage of dc link in multi-machine power system.

Fig. 17.   Voltage of G3 in multi-machine power system.

was performances to verify the result. Our main conclusions include:

1) Based on the sensitivity analysis, it is clear that the sensitivities among the control parameters are different, which can provide information to choose the dominate control parameters, i.e., the UDCP of the WT system controller can be identified.

2) By using PSO to optimize the UDCP, the computational time can be reduced compare with optimizing all the control parameters simultaneous. The efficiency of optimization can be improved.

3) Simulation results have shown that our approach of using UDCP only is similar with using the optimized all control parameters. This means our UDCP approach will not only be able to improve the dynamic performance of WT system leading enhanced fault ride-through capability, but it can also reduce the computational cost since we only need to optimize the selected UDCP parameters.

There are several interesting future research directions along this topic. For instance, in our current work, we only choose a small range of the control parameters for small signal stability analysis. We would like to note that it is possible that the PI controller may have a large range of parameters under different system situations. Therefore, it would be interesting to extend this work to consider large change sensitivity analysis with a wide range of control parameter variations. Also, as indicated in [31], the large signal stability analysis is also of critical importance in power system stability analysis. The control parameters sensitivity analysis based on large signal stability analysis could be used for controller design based on Lyapunov-based techniques [32]. Furthermore, the wind turbine system we considered in our current work is relatively small. Nevertheless, the proposed method could be a good initial study of computation effort reduction issue. A typical system curve for multiple DFIGs trajectory sensitivity analysis will be needed to handle large-scale wind farms. Meanwhile, from the DFIG modeling side, in our current study we represent multiple DFIGs as one WT in modeling and simulation. While this is a common practice and reasonable simplification in the research community because there is normally no mutual interactions between wind turbines on a wind farm [20], we would like to note that it would be important to consider more close-to-reality multiple DFIG models in order to demonstrate the feasibility of such control approaches to facilitate realistic grid connected wind farm development.

REFERENCES

[1] U.S. Department of Energy, "The smart grid: An introduction," 2008.
[2] A. Ipakchi and F. Albuyeh, "Grid of the future," *IEEE Power Energy Mag.*, vol. 7, pp. 52–62, 2009.
[3] IEEE Smart Grid Initiative [Online]. Available: http://smartgrid.ieee.org/
[4] European Commission, "European smart grids technology platform," 2006.
[5] A. Grauers, "Efficiency of three wind energy generator system," *IEEE Trans. Energy Convers.*, vol. 11, pp. 650–657, 1996.
[6] R. Pena, J. C. Clear, and G. M. Asher, "Doubly fed induction generator using back-to-back PWM converters and its application to variable-speed wind energy generation," *IEE Proc. Elec. Power Appl.*, vol. 143, pp. 231–241, 1996.
[7] F. Wu, X. P. Zhang, K. Godferey, and P. Ju, "Small signal stability analysis and optimal control of a wind turbine with doubly fed induction generator," *IET Gener., Transm., Distrib.*, vol. 1, pp. 751–760, 2007.
[8] L. Yang, G. Y. Yang, Z. Xu, Z. Y. Dong, K. P. Wong, and X. Ma, "Optimal controller design of a doubly-fed induction generator wind turbine system for small signal stability enhancement," *IET Gener., Transm., Distrib.*, vol. 5, pp. 579–597, 2010.
[9] P. J. Werbos, "Computational intelligence for the smart grid-history, challenges, and opportunities," *IEEE Comput. Intel. Mag.*, vol. 6, no. 3, pp. 14–21, 2011.
[10] G. K. Venayagamoorthy, "Dynamic, stochastic, computational, and scalable technologies for smart grids," *IEEE Comput. Intel. Mag.*, vol. 6, no. 3, pp. 22–35, 2011.
[11] W. Qiao, R. G. Harley, and G. K. Venayagamoorthy, "Coordinated reactive power control of a large wind farm and a STATCOM using heuristic dynamic programming," *IEEE Trans. Energy Convers.*, vol. 24, no. 2, pp. 493–503, 2009.

[12] W. Qiao, G. K. Venayagamoorthy, and R. G. Harley, "Real-time implementation of a STATCOM on a wind farm equipped with doubly fed induction generators," *IEEE Trans. Ind. App.*, vol. 45, no. 1, pp. 98–107, Jan./Feb. 2009.

[13] H. L. Xie, P. Ju, J. Luo, Y. Ning, H. Zhu, and X. Wang, "Identifiability analysis of load parameters based on sensitivity calculation," *Autom. Elec. Power Syst.*, vol. 33, pp. 17–21, 2009.

[14] T. Smed, "Feasible eigenvalue sensitivity for large power systems," *IEEE Trans. Power Syst.*, vol. 8, pp. 555–563, 1993.

[15] H. K. Nam and Y. K. Kim, "A new eigen-sensitivity theory of augmented matrix and it's applications to power system stability," *IEEE Trans. Power Syst.*, vol. 15, pp. 363–369, 2000.

[16] K. W. Wang and C. Y. Chung, "Multi-machine eigenvalue sensitivities of power system parameters," *IEEE Trans. Power Syst.*, vol. 15, pp. 741–747, 2000.

[17] L. H. Yang, Z. Xu, J. Østergaard, Z. Y. Dong, K. P. Wong, and X. Ma, "Oscillatory stability and eigenvalue sensitivity analysis of a DFIG wind turbine system," *IEEE Trans. Energy Convers.*, vol. 26, pp. 328–339, 2011.

[18] A. D. Hansen, P. Sørensen, F. Iov, and F. Blaabjerg, "Control of variable speed wind turbines with doubly-fed induction generators," *Wind Eng.*, vol. 28, no. 4, pp. 411–434, 2004.

[19] R. Aghatehrani and R. Kavasseri, "Reactive power management of a DFIG wind system in micro-grids based on voltage sensitivity analysis," *IEEE Trans. Sustainable Energy*, vol. 2, pp. 451–458, 2010.

[20] V. Akhmatov, "Analysis of dynamic behavior of electric power systems with large amount of wind power," Ph. D, Tech. Univ. Denmark, Kgs, Lyngby, Denmark, 2003.

[21] P. Ju and D. Q. Ma, *Identification of Power Load*, 2nd ed. Beijing, China: China Electric Power Press, 2008.

[22] J. Kennedy and R. Eberhart, "Particle swarm optimization," in *Proc. IEEE Int. Conf. Neural Netw.*, Perth, Australia, 1995, vol. IV, pp. 1942–1948.

[23] Y. D. Valle, G. K. Vanayagamoorthy, S. Mohagheghi, J. C. Hernandez, and R. D. Harley, "Particle swarm optimization: Basic concepts, variants and applications in power systems," *IEEE Trans. Evol. Comput.*, vol. 12, no. 2, pp. 171–195, Apr. 2008.

[24] F. Wu, X. P. Zhang, P. Ju, and M. J. H. Sterling, "Decentralized nonlinear control of wind turbine with doubly fed induction generator," *IEEE Trans. Power Syst.*, vol. 23, no. 2, pp. 613–621, 2008.

[25] W. Qiao, G. K. Venayagamoorthy, and R. G. Harley, "Design of optimal PI controllers for doubly fed induction generators driven by wind turbines using particle swarm optimization," in *Proc. Int. Joint Conf. Neural Netw.*, 2006, pp. 1982–1987.

[26] W. Qiao, J. Liang, G. K. Venayagamoorthy, and R. G. Harley, "Computational intelligence for control of wind turbine generators," in *Proc. Power Energy Soc. Gen. Meet.*, 2011, pp. 1–6.

[27] *MATLAB User's Guide—Dynamic System Simulation for MATLAB* The Math Works Inc..

[28] A. Mendonca and J. A. P. Lopes, "Robust tuning of power system stabilisers to install in wind energy conversion systems," *IET Renewable Power Gener.*, vol. 3, no. 4, pp. 465–475, 2009.

[29] N. Kshatriya, U. D. Annakkage, F. M. Hughes, and A. M. Gole, "Optimized partial eigenstructure assignment-based design of a combined PSS and active damping controller for a DFIG," *IEEE Trans. Power Syst.*, vol. 25, no. 2, pp. 866–876, 2010.

[30] H. Huang and C. Y. Chung, "Coordinated damping control design for DFIG-based wind generation considering power output variation," *IEEE Trans. Power Syst.*, vol. 27, no. 4, pp. 1916–1925, 2012.

[31] D. Marx, P. Magne, B. Nahid-Mobarakeh, S. Pierfederici, and B. Davat, "Large signal stability analysis tools in DC power systems with constant power loads and variable power loads—a review," *IEEE Trans. Power Electron.*, vol. 27, no. 4, pp. 1773–1787, 2012.

[32] P. Kundur, *Power System Stability and Control*. New York: McGraw-Hill, 1994.

Yufei Tang received the B.Eng. and M.Eng. degrees in electrical engineering from Hohai University, Nanjing, China, in 2008 and 2011, respectively, and is currently working toward the Ph.D. degree in the Department of Electrical, Computer, and Biomedical Engineering, University of Rhode Island, Kingston.

His research interests include power system modeling, power system stability control, wind energy generation and integration, smart grid, and the application of computational intelligence in power systems.

Ping Ju (SM'10) received the B.Eng. and M.S. degrees in electrical engineering from Southeast University, China, in 1982 and 1985, respectively, and the Ph.D. degree in electrical engineering from Zhejiang University, Hangzhou, China, in 1988.

From 1994 to 1995, he was an Alexander-von-Humboldt Fellow at the University of Dortmund, Germany. He is now a Professor in Electrical Engineering at HoHai University, Nanjing, China. His research interests include modeling and control of power systems, and smart grid with renewable power generation. He has published 4 research books, and authored and co-authored over 200 journal papers.

Dr. Ju received the Scientific Funds for Outstanding Young Scientists of China.
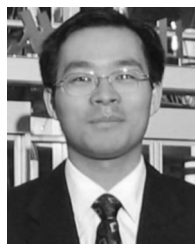
Haibo He (SM'11) received the B.S. and M.S. degrees in electrical engineering from Huazhong University of Science and Technology (HUST), Wuhan, China, in 1999 and 2002, respectively, and the Ph.D. degree in electrical engineering from Ohio University, Athens, in 2006.

From 2006 to 2009, he was an Assistant Professor in the Department of Electrical and Computer Engineering, Stevens Institute of Technology, Hoboken, NJ. He is currently an Associate Professor in the Department of Electrical, Computer, and Biomedical Engineering at the University of Rhode Island, Kingston. His research interests include smart grid, adaptive dynamic programming (ADP), computational intelligence, cybersecurity, and hardware design for machine intelligence. He has published one research book (Wiley), edited 6 conference proceedings (Springer), and authored and co-authored over 100 peer-reviewed journal and conference papers. Dr. He's researches have been covered by numerous media such as IEEE *Smart Grid Newsletter*, *The Wall Street Journal*, and *Providence Business News*. Currently, he is an Associate Editor of the IEEE TRANSACTIONS ON NEURAL NETWORKS AND LEARNING SYSTEMS, and IEEE TRANSACTIONS ON SMART GRID. He received the National Science Foundation (NSF) CAREER Award (2011) and Providence Business News (PBN) Rising Star Innovator Award (2011).

Chuan Qin received the B.S. degree from Nantong Institute of Technology, Nantong, China, in 2002 and the M.S. degree from Hohai University, Nanjing, China, in 2005. He is now working toward the Ph.D. degree in electrical engineering at Hohai University, China.

Currently, he is also a lecture in the College of Energy and Electrical Engineering at Hohai University. His research interests include modeling and control of the renewable energy generation.

Feng Wu received the B.Eng and M.S. degrees in electrical engineering from HoHai University, China, in 1998 and 2002, respectively, and the Ph.D. degree from the University of Birmingham, U.K., in 2009.

Currently, he is a Professor in electrical engineering within the college of Energy and Electrical Engineering at Hohai University, China. His research interest is modeling and control of renewable energy generation systems. He has authored and coauthored over 30 journal and conference papers.